

Behaviors of Martian CO₂-driven dry climate system and conditions for atmospheric collapses

Yasuto Watanabe^{1,†,*}, Eiichi Tajika¹, Arihiro Kamada²

¹Department of Earth and Planetary Science, Graduate School of Science, The University of Tokyo, Tokyo, Japan

²Department of Geophysics, Graduate School of Science, Tohoku University, Sendai, Japan

[†]Present affiliation: Meteorological Research Institute, Japan Meteorological Agency, Tsukuba, Japan

*Corresponding author: Yasuto Watanabe (yasuto.watanabe.wess@gmail.com). Department of Atmosphere, Ocean, and Earth System Modeling Research, Meteorological Research Institute, Japan Meteorological Agency. 1-1 Nagamine, Tsukuba, Ibaraki, Japan. Tel. +81-29-853-8648

Abstract

The present Martian climate is characterized by a cold and dry environment with a thin atmosphere of carbon dioxides (CO₂). In such conditions, the planetary climate and habitability are determined by the distribution of CO₂ between exchangeable reservoirs, that is the atmosphere, ice caps, and regolith. This produces unique responses of the Martian CO₂-driven climate system to variations of astronomical forcings. Specifically, it has been shown that the phenomenon called an atmospheric collapse occurs when the axial obliquity is low, affecting the Martian climatic evolution. However, the behavior of the Martian climate system and the accompanying changes in climate and habitability of such planets remain ambiguous. Here we employed a latitudinally-resolved Martian energy balance model and assessed the possible climate on Mars for wider ranges of orbital parameters, solar irradiance, and total exchangeable CO₂ mass. We show that the atmospheric collapse occurs when the obliquity is below $\sim 10^\circ$ when other parameters are kept at the present Mars condition. We also show that the climate solutions on Mars depend on orbital parameters, solar luminosity, and the total exchangeable CO₂ mass. We found that the atmospheric collapse would have occurred repeatedly in the history of Mars following the variation of the axial obliquity, while the long-term evolution of atmospheric $p\text{CO}_2$ is also affected by the changes in the total exchangeable CO₂ mass in Martian history. Even considering the broad ranges of these parameters, the habitable conditions in the Martian CO₂-driven dry climate system would be limited to high-latitude summers.

Keywords

Mars; climate; atmospheric collapse; obliquity

Highlights

- Atmospheric collapse occurs under obliquity lower than $\sim 10^\circ$ on the present Mars.
- Atmospheric collapses would have occurred repeatedly in the history of Mars.
- Habitability on Martian CO₂-driven dry climate systems would be limited.

Introduction

The climate of the present Mars is characterized by cold and dry conditions. Most of the surface H_2O is located at the polar caps and the subsurface and CO_2 also condenses into the surface at high latitudes. There is no active volcanism and plate tectonics on the present Mars, meaning that the carbonate-silicate geochemical cycle, a negative feedback that stabilizes the atmospheric $p\text{CO}_2$ and climate in Earth's history (Walker et al. 1981), does not operate on present Mars. In such conditions, the Martian atmospheric $p\text{CO}_2$ and the climate are controlled by the equilibrium among the three exchangeable surface reservoirs of CO_2 , that is, atmosphere, polar ice caps, and regolith (Gierasch and Toon 1973; Toon et al. 1980; McKay et al. 1991; Zent and Quinn 1995; Nakamura and Tajika 2003; Manning et al. 2006; Haberle et al. 2017; Jakosky and Edwards 2018; Buhler and Piqueux 2021). CO_2 condenses to the surface at high latitudes in winter and it sublimates into the atmosphere during the spring and the summer. Atmospheric CO_2 is also adsorbed by the surface regolith layer (Fanale and Cannon 1974; Toon et al. 1980; Fanale and Salvail 1982; Kahn 1985; Zent and Quinn 1995). The distribution of CO_2 among these surface reservoirs and climatic conditions are controlled by a thermodynamic balance between these surface reservoirs. This Martian CO_2 -dominated climate system has two different stable steady states of climate modes under the present condition (Fanale and Salvail 1982; McKay et al. 1991; Haberle et al. 1994; Nakamura and Tajika 2001, 2002): one is the permanent-ice climate mode in which the atmospheric $p\text{CO}_2$ is controlled primarily by the thermodynamic balance between atmosphere and a permanent CO_2 ice and the other is the climate mode without a perennial CO_2 ice. It is noteworthy that, under the permanent-ice climate mode, the surface pressure is kept especially low because most CO_2 is partitioned into the CO_2 ice, hence the formation of permanent ice causes an event called “atmospheric collapse” (McKay et al. 1991; Haberle et al. 1994; Nakamura and Tajika 2002; Kreslavsky and Head 2005; Soto et al. 2015). Indeed, the time-dependent calculations of the Martian recent past indicate an occurrence of atmospheric collapse (Manning et al. 2006, 2019). Therefore, the behavior of the Martian CO_2 climate system is critical for understanding the evolution of the Martian surface environment.

One of the critical factors that affect the behavior of the Martian CO₂ climate system is the variations of orbital parameters (Toon et al. 1980; Nakamura and Tajika 2003; Kite et al. 2013, 2017; Soto et al. 2015; Batalha et al. 2016; Hayworth et al. 2020). It is well known that the variations of orbital parameters caused the quasi-periodic glacial-interglacial climate changes during the Quaternary on Earth (Hays et al. 1976; Raymo 1997; Huybers 2011; Abe-Ouchi et al. 2013; Watanabe et al. 2023). The variation of orbital parameters on Mars, especially that of obliquity, is characterized by its large amplitude of variations owing to the lack of a large moon (Laskar et al. 2004), which would have reached $\sim 0^\circ$ and $\sim 60^\circ$ in the past (Laskar et al. 2004) (Figure 1). The variation of obliquity modifies the latitudinal-seasonal distribution of the insolation received on the Martian surface (Toon et al. 1980; Nakamura and Tajika 2003; Soto et al. 2015). Specifically, the atmospheric collapse may have occurred when the obliquity was low in the recent past (Nakamura and Tajika 2003; Manning et al. 2006). This may have formed the layered deposits in the polar ice caps (Hvidberg et al. 2012; Bierson et al. 2016; Smith et al. 2016; Becerra et al. 2016, 2017, 2019; Lalich and Holt 2017; Manning et al. 2019; Lalich et al. 2019), surface deposits (Schon et al. 2009; Bernhardt et al. 2019), glaciers (Forget et al. 2006; Bramson et al. 2017; Dundas et al. 2018), and/or gullies at the mid-latitudes (Costard et al. 2002; Head et al. 2003; Conway et al. 2019).

In the more distant past, the solar irradiance and the total amount of exchangeable CO₂ would have been important in regulating the Martian climate. The solar luminosity was $\sim 30\%$ dimmer at ~ 4.5 Ga than the present brightness (Gough 1981). On the other hand, it has been suggested that there would have been an ocean on early Mars (Head et al. 1999; Citron et al. 2018), indicating a strong greenhouse effect for sustaining liquid water on the surface and dynamical climate evolution on early Mars (Batalha et al. 2016; Rapin et al. 2023; Kite and Conway 2024). The total exchangeable CO₂ must have been much higher on early Mars than on the present Mars. This would have helped warm the Martian surface by elevating the atmospheric $p\text{CO}_2$, while very high atmospheric $p\text{CO}_2$ would have promoted the formation of CO₂ clouds in the polar region (Kasting 1991; Pierrehumbert and Erlick 1998), potentially limiting the warming effect of CO₂. The total exchangeable CO₂ has

decreased owing to the deposition of carbonates and escape to space via ion sputtering and photochemical escape (Kahn 1985; Haberle et al. 1994; Jakosky et al. 1994; Manning et al. 2006; Kurahashi-Nakamura and Tajika 2006; Hu et al. 2015). For a better constraint on the evolutionary path of the Martian climate, the behavior of the Martian CO₂ climate system to different values of orbital parameters, solar luminosity, and total mass of CO₂ is critical. However, the dependency of the climate mode for Mars and Mars-like exoplanets has been studied only for a very limited range of parameters (Nakamura and Tajika 2001, 2002, 2003; Soto et al. 2015). Here we employ a one-dimensional energy balance model and assess the multiple climate modes on Mars and Mars-like planets with different total exchangeable CO₂, solar irradiance, obliquity, precession, and eccentricity. We discuss possible Martian climate modes for wider ranges of parameters, considering Mars-like exoplanets which have a CO₂-dominated climate system similar to that of Mars, and discuss the habitability of such planets. We further show the condition of the atmospheric collapse on Mars and the time-dependent behavior of the atmospheric collapse.

Method

One-dimensional energy balance model

We used a latitudinally-resolved energy-balanced climate model (EBM) for Mars (Nakamura and Tajika 2003) (Figure 2). This model calculates the exchange of energy at the planetary surface and atmospheric layers and the exchange of CO₂ between the atmosphere, surface CO₂ ice, and surface regolith. The meridional resolution of the model is 2°. In each grid, the atmosphere is divided into four layers that have an equal amount of atmosphere. CO₂ condensates onto the surface of each grid when the surface temperature is below the sublimation temperature. The balances of energy of the surface and atmospheric layers are represented as follows:

$$C_g \frac{dT}{dt} = (1 - \alpha) \cdot S + F_{ira,g} - F_{ire,g} - F_{sbl} + F_{lat} \quad (1)$$

$$C_a \frac{dT_{a,1}}{dt} = F_{ira,a1} - F_{ire,a1} + F_{sbl} + F_{adv,a1} \quad (2)$$

$$C_a \frac{dT_{a,i}}{dt} = F_{ira,ai} - F_{ire,ai} + F_{adv,ai} \quad (i = 2, 3, 4) \quad (3)$$

where the subscript g and a represent the ground layer and the atmospheric layer, respectively; the subscript number represents the number of the atmospheric layer (bottom layer is 1); T is the temperature; C_g and C_a are the heat capacity of the ground and each atmospheric layer ($C_g = 1.0 \times 10^7 \text{ J m}^{-2} \text{ K}^{-1}$), respectively (Nakamura and Tajika 2003); S is the solar irradiance; α is the surface albedo; F_{ire} and F_{ira} are the emission and absorption flux of infrared radiation, respectively; F_{sbl} and F_{lat} are the sensible and latent heat flux, respectively.

In this model, we introduced the effect of the topographic dichotomy of Mars. The local surface pressure ($P_{atm,topo}$) is calculated as follows:

$$P_{atm,topo} = P_{atm} \cdot \exp\left(-\frac{z}{H_1}\right) \quad (4)$$

where P_{atm} is the global-mean atmospheric $p\text{CO}_2$, z is the surface altitude relative to the mean topographic height of Mars, and H_1 is the local scale height of the atmospheric bottom layer, which is calculated assuming the hydrostatic equilibrium:

$$H_1 = \frac{kT_{a,1}}{mg} \quad (5)$$

where k is the Boltzmann constant, m is the mean mass of the atmosphere (i.e., CO_2) ($m = 0.044 \text{ kg mol}^{-1}$), and g is the gravitational acceleration of Mars. The latitudinal mean topography of Mars is created using the dataset of the Mars Global Surveyor's Mars Orbiter Laser Altimeter (MOLA) (Zuber et al. 1992; Smith et al. 2001), MOLA Mission Experiment Gridded Data Records (MEGDRs).

The horizontal thermal advection terms in the atmospheric layer are represented as follows:

$$F_{adv,a,j} = \frac{D_j}{4(\Delta\Phi)^2 \cos(lat_j)} (\cos(\phi_{h,j+1}) \cdot (T_{a,j+1} - T_{a,j}) - \cos(\phi_{h,j}) \cdot (T_{a,j} - T_{a,j-1})) \quad (6)$$

Where j is the latitudinal grid number ($j = 1, 2, \dots$) and φ is the latitude. The diffusion coefficient D is calculated as follows:

$$D = D_0 \cdot P_{atm,topo}, \quad (7)$$

where D_0 is the diffusion coefficient at $P_{atm,topo}$ of 1 bar ($D_0 = 0.7$) (Stone 1972; Hoffert et al. 1981). The sensible heat flux is calculated as follows (Gierasch and Toon 1973; Yokohata et al. 2002; Nakamura and Tajika 2003):

$$F_{sbl} = k_{sbl,0} \cdot P_{atm,topo} \cdot \frac{T_g - T_{a1}}{T_{a1}} \quad (8)$$

where $F_{sbl,0}$ is the reference sensible heat flux ($k_{sbl,0} = 2.04 \times 10^3 \text{ W m}^{-2} \text{ bar}^{-1}$) (Nakamura and Tajika 2003). The long-wave emission flux from the ground and each atmospheric layer are calculated as follows:

$$F_{ire,g} = \epsilon_g \sigma T_g^4 \quad (9)$$

$$F_{ire,ai} = 2\epsilon_a \sigma T_{a,i}^4 \quad (i = 1, 2, 3, 4) \quad (10)$$

where σ is the Stefan-Boltzmann constant ($5.67 \times 10^{-8} \text{ W m}^{-2} \text{ K}^{-4}$) and ϵ_g is the ground emissivity ($\epsilon_g = 1$). The atmospheric emissivity (ϵ_a) is parameterized to fit the surface temperature estimated by a previous study (Pollack et al. 1987), as follows:

$$\epsilon_a = \epsilon_{a1}y^5 + \epsilon_{a2}y^4 + \epsilon_{a3}y^3 + \epsilon_{a4}y^2 + \epsilon_{a5}y + \epsilon_{a6} \quad (P_{atm,topo} \geq 0.0004 \text{ bar}) \quad (11)$$

$$\epsilon_a = \frac{P_{atm,topo}}{0.0004 \text{ bar}} \cdot \epsilon_a(P_{atm,topo} = 0.0004 \text{ bar}) \quad (P_{atm,topo} < 0.0004 \text{ bar})$$

where y represents $\log(P_{atm,topo})$ and ϵ_{a0} , ϵ_{a1} , ϵ_{a2} , ϵ_{a3} , ϵ_{a4} , ϵ_{a5} , and ϵ_{a6} are 0.0004, 0.009, 0.0792, 0.3324, 0.6782, and 0.5667, respectively. Using these values, F_{ira} is represented as follows:

$$F_{ira,g} = \epsilon_g \cdot \epsilon_a \cdot (1 - \epsilon_a)^{j-1} \sigma T_{aj}^4 \quad (12)$$

$$F_{ira,ai} = F_{ira,ai\downarrow} + F_{ira,ai\uparrow} \quad (13)$$

The absorption fluxes of the downward and upward long-wave radiations in each atmospheric layer are represented as follows:

$$F_{ira,ai\downarrow} = \sum_{k=i+1,\dots,4} [\epsilon_a (1 - \epsilon_a)^{k-i-1} \sigma T_{ak}^4] \quad (i = 1, 2, 3) \quad (14)$$

$$F_{ira,ai\downarrow} = 0 \quad (i = 4) \quad (15)$$

$$F_{ira,ai\uparrow} = \epsilon_g \sigma T_g^4 \quad (i = 1) \quad (16)$$

$$F_{ira,ai\uparrow} = \epsilon_g (1 - \epsilon_a)^{i-1} \sigma T_g^4 + \sum_{k=1, \dots, i-1} [\epsilon_a (1 - \epsilon_a)^{i-k-1} \sigma T_{ak}^4] \quad (i = 2, 3, 4) \quad (17)$$

where the subscripts \downarrow and \uparrow represent the absorption fluxes of downward and upward long-wave radiations, respectively.

The heat capacity of each atmospheric layer is calculated as follows:

$$C_a = 0.25 \cdot C_{a,0} \cdot P_{atm,topo} \quad (18)$$

where $C_{a,0}$ is the heat capacity of the atmosphere at 1 bar ($C_{a,0} = 2.3 \times 10^7 \text{ J m}^{-2} \text{ K}^{-1}$) (Nakamura and Tajika 2003). Note that the factor 0.25 is multiplied to divide the atmosphere into four layers that have an equal atmospheric mass. The surface albedos of the grid without and with CO_2 ice are defined here as α_g and α_i , respectively, and represented as follows:

$$\begin{aligned} \alpha_g &= \alpha_{g1}y^5 + \alpha_{g2}y^4 + \alpha_{g3}y^3 + \alpha_{g4}y^2 + \alpha_{g5}y + \alpha_{g6} \quad (P_{atm,topo} > 0.001 \text{ bar}) \\ &= \alpha_{g0} \quad (P_{atm,topo} \leq 0.001 \text{ bar}) \end{aligned} \quad (19)$$

$$\begin{aligned} \alpha_i &= \alpha_{i1}y^3 + \alpha_{i2}y^2 + \alpha_{i3}y + \alpha_{i4} \quad (P_{atm,topo} > 0.001 \text{ bar}) \\ &= \alpha_{i0} \quad (P_{atm,topo} \leq 0.001 \text{ bar}) \end{aligned} \quad (20)$$

where α_{g0} , α_{g1} , α_{g2} , α_{g3} , α_{g4} , α_{g5} , and α_{g6} are 0.21, -0.0008 , -0.0074 , -0.0147 , 0.0337, 0.1381, and 0.3249, respectively, and α_{i0} , α_{i1} , α_{i2} , α_{i3} , and α_{i4} are 0.4, 0.0029, 0.0232, 0.0598, and 0.45, respectively. The CO_2 -dependence of the surface albedo represents the effect of Rayleigh scattering when $P_{atm,topo}$ is high. This parameterization is based on Nakamura and Tajika (2003), but the values of α_{i0} and α_{i4} are lowered from the original values (0.7 and 0.75, respectively) to fit the timings of the appearance and disappearance of polar CO_2 ice caps. The updated values are consistent with those estimated from recent observations (Gary-Bicas et al. 2020). We note here that we do not consider the effect of H_2O ice on the surface albedo because our focus is to assess the behavior of the Martian CO_2 -driven climate system. This may lead to the overestimation of the surface temperature especially

at the poles and underestimation of the size of the surface CO₂ ice reservoir when the obliquity is low: however, we expect that this would not strongly modify the behavior of CO₂ investigated in this study.

Condensation of CO₂ to the surface

The condensation of CO₂ ice to the surface occurs when the surface temperature drops below the sublimation temperature. Similarly, the sublimation of CO₂ ice from the surface occurs when the surface temperature exceeds the sublimation temperature. The model first estimates the energy balance without latent heat of the atmospheric CO₂ condensation ($F_{\text{lat}} = 0$). If the surface temperature drops below the sublimation temperature, atmospheric CO₂ condenses at the surface, and the amount of condensed CO₂ at the time step is calculated as follows:

$$\Delta P_{ice} = - \frac{[(1-\alpha) \cdot S + F_{ira,g} - F_{ire,g} - F_{sbl}] - C_g \cdot (T_{sub} - T'_g)}{L} \quad (21)$$

where L is the latent heat and T'_g is the surface temperature calculated with a F_{lat} of zero. The CO₂ sublimation temperature (T_{sub}) is represented as follows (Nakamura and Tajika 2003):

$$T_{sub} = T_{sub,4}y^4 + T_{sub,3}y^3 + T_{sub,2}y^2 + T_{sub,1}y + T_{sub,0}, \quad (22)$$

where ($T_{sub,0}$, $T_{sub,1}$, $T_{sub,2}$, $T_{sub,3}$, $T_{sub,4}$) is (194.36, 26.451, 2.8593, 0.1814, 0.0046).

Adsorption of CO₂ to surface regolith

We estimated the size of the regolith reservoir using the formulation of Nakamura and Tajika (2001; 2002).

$$P_{reg} = \int_{-\pi/2}^{\pi/2} K_{reg} \exp\left(-\frac{T}{T_d}\right) P_{atm,topo}^\gamma \cos(\phi) d\phi, \quad (23)$$

where K_{reg} is the tuning factor to reproduce the present regolith reservoir size ($K_{reg} = 72.8 \text{ bar}^{-\gamma}$), T_d is 35 K, and γ is 0.275. The value of K_{reg} was tuned so that the model reproduces the present atmospheric $p\text{CO}_2$ (6 mbar) under the present exchangeable CO₂ reservoir size (53.88 mbar) (Hu et al., 2015). Because the timescale for the equilibrium of the regolith reservoir would be much longer

than the Martian year (Kieffer and Zent 1992), the behavior of the regolith reservoir is treated differently. The model calculates the annual-mean temperature and atmospheric $p\text{CO}_2$ of each grid by averaging the temperature and atmospheric $p\text{CO}_2$ of the grid in the past time steps corresponding to one Martian year, which is saved in the model at every 5 time steps. Finally, the total exchangeable CO_2 reservoir size (P_{tot}) is represented as follows:

$$P_{\text{tot}} = P_{\text{atm}} + P_{\text{ice}} + P_{\text{reg}}, \quad (24)$$

where P_{atm} and P_{ice} are the mass of CO_2 in the atmosphere and surface CO_2 ice, respectively.

Definition of the habitability of the surface

We examined the surface area fraction of habitable conditions, defined here as conditions for liquid water to be able to exist ($T > 273$ K) in a year and/or in the area on a planet. In order to quantify the habitability of Mars, we adopted the concept of net fractional habitability, a fraction of the surface area or the orbit of a planet that might be habitable (i.e., surface temperatures between 273 K and 373 K) (Spiegel et al. 2008):

$$f_{\text{hab}} = \frac{1}{t_{\text{year}}} \int_{-\pi/2}^{\pi/2} \left\{ \int_0^P H(\phi, t) \cdot dt \right\} \cos \phi d\phi, \quad (25)$$

where t_{year} is the length of the year and H is the habitability function. The habitability function is represented as follows:

$$\begin{aligned} H(\phi, t) &= 1 \quad (273 \leq T(\phi, t) \leq 373) \\ &= 0 \quad (T(\phi, t) < 273 \text{ or } T(\phi, t) > 373). \end{aligned} \quad (26)$$

We note here that we assumed that there is only a small amount of H_2O that does not affect the general behavior of the CO_2 -driven dry climate system in the surface environment as in the present Mars.

Experimental setup

We conducted numerical experiments under various total exchangeable CO₂ (i.e., exchangeable amounts of CO₂ in the surface reservoirs), orbital parameters (obliquity, precession angle from the vernal equinox, and eccentricity), and solar luminosity and assessed the existence of the multiple equilibriums of Mars. We varied one of these parameters from the present Mars condition. We further conducted calculations with varying a set of obliquity and P_{tot} , under the solar luminosities of 1.00 and 0.75 times relative to the present value. We also varied a set of solar luminosity and P_{tot} under the obliquity of 10°. We further conducted a series of experiments assuming different ages. In this series of experiments, we changed the solar luminosity and the exchangeable CO₂ reservoir size. The solar luminosity is calculated as follows (Gough 1981; Feulner 2012) (Figure 3a):

$$S^* = \frac{5}{2 \cdot (\frac{\text{Age}_{\text{Ga}}}{4.57}) + 5} \quad (27)$$

where S^* is the solar luminosity relative to the present and Age_{Ga} is the age in Ga ($\text{Age}_{\text{Ga}} = 0$ Ga at the present). The total exchangeable CO₂ reservoir size is estimated based on the previous study considering the escape of CO₂ to space and the deposition of CO₂ as carbonates (Hu et al. 2015) (Figure 3b).

In addition, we have conducted a set of calculations with idealized variations of the obliquity to elucidate the response of the atmosphere–ice cap system. For these experiments, we assumed artificial variations of Martian obliquity, which varies between 5 and 35° with a cosine curve, with different periods (10, 20, 30, 60, and 100 kyr). The values of other orbital parameters are fixed at the present Martian value. For this calculation, the regolith reservoir is not coupled to the model because our model cannot simulate the transient response of the regolith reservoir. The total exchangeable CO₂ reservoir is set to 0.1 bar in this experiment.

Results

Reproduction of the present Martian condition

The results for the present Mars condition are shown in Figure 4. The simulated seasonal variation of the surface temperature is broadly consistent with the simulations by three-dimensional general circulation models (Toon et al. 1980; Pollack et al. 1981, 1990, 1993; Wood and Paige 1992) (Figure 4b). The seasonal variations of the surface pressure near the landing site of Viking 1 and 2 show that the variations of the atmospheric $p\text{CO}_2$ from the winter to summer of the northern hemisphere are slightly underestimated (Figure 4d). This would be attributed to the treatment of albedo of the CO_2 ice: the observed values are different between hemispheres, while the model assumes an equivalent value for both hemispheres. In our model, the permanent CO_2 ice does not form in the present Martian condition. The present Martian condition is reproduced with a total exchangeable reservoir size of ~ 0.054 bar, most of which is distributed to the surface regolith layer. The present observation of the Martian poles indicates that there is virtually no CO_2 ice (Kieffer 1979; Byrne 2009; Titus and Cushing 2014; Piqueux et al. 2015; Haberle et al. 2017). Although it sometimes remains in summer, we expect that this would be associated with the local topographic structure, and the behaviors of the present Martian would be sufficient for representing the fundamental behavior of the Martian CO_2 -driven climate system as shown in this study.

Behaviors of the Martian climate system under different climate forcings

We show the dependency of the steady states of the Martian climate system on different values of obliquity in Figure 5a–5c. When the obliquity changes from the present value (25.19°), the global mean surface temperature does not strongly shift from the present value (200–210 K). When obliquity is below a critical value ($\sim 12^\circ$), permanent ice forms in high-latitude regions. This boundary is broadly consistent with the estimate based on three-dimensional AGCM (Soto et al. 2015). When the obliquity is 12° , the permanent ice exists only in the north pole, while the permanent ice forms in the south pole when obliquity is below 10° and atmospheric $p\text{CO}_2$ becomes small. With the permanent CO_2 ice in

both hemispheres, the CO₂ ice cap reservoir gradually becomes the primary exchangeable CO₂ reservoir as the obliquity becomes small. This is because the size of the regolith reservoir decreases following the decline in the atmospheric $p\text{CO}_2$. This behavior is similar to the estimates by the other theoretical model (Buhler and Piqueux 2021). The minimum temperature of the planetary surface also becomes lower following the decline in the sublimation temperature owing to the lowering atmospheric $p\text{CO}_2$. When the obliquity is higher than the present value, the atmospheric $p\text{CO}_2$ does not strongly respond to the increase of obliquity, which is different from the result of the previous study that suggests a stronger sensitivity of atmospheric $p\text{CO}_2$ to the increase of obliquity (Buhler and Piqueux 2021).

The seasonal and latitudinal distributions of the surface temperature for different obliquities are shown in Figure 4b and 6. When the obliquity is lower than $\sim 28^\circ$ (Figure 5b), the highest surface temperature is achieved at low-latitude regions (red dots in Figure 5c and Figure 6a). In this condition, the maximum surface temperature is around 240 K (Figure 5b), which is below the freezing point of water. The maximum surface temperature increases owing to an increase in the obliquity when obliquity is over $\sim 28^\circ$ because the insolation at high-latitude regions becomes higher than in low-latitude regions, leading to the high summer temperature (Figure 6c). Under the obliquity higher than $\sim 35^\circ$, some parts of high-latitude regions become warmer than the freezing point of water during summer (Figure 5b), meaning that this region is at least seasonally habitable. However, the habitable condition is limited to only high-latitude regions on the surface during summer.

The responses of the distribution of CO₂ and the surface temperature to different total exchangeable CO₂ (P_{tot}) under the present Martian orbital parameters are summarized in Figure 7a–7c. When P_{tot} is below ~ 130 mbar, the regolith reservoir is the dominant CO₂ reservoir as in the case of the present Mars (Figure 7a). When P_{tot} is over ~ 130 mbar, the atmosphere becomes the dominant CO₂ reservoir. The CO₂ ice cap reservoir was small compared with atmosphere and regolith reservoirs at any P_{tot} . The size of the regolith reservoir increases following the increase of P_{tot} when P_{tot} is below ~ 130 mbar, while it becomes less sensitive to P_{tot} when P_{tot} is over ~ 130 mbar, at which the regolith

reservoir size is ~ 50 mbar. The atmospheric CO_2 reservoir, on the other hand, correlates positively to P_{tot} at any P_{tot} explored in Figure 7a. As a result, the global annual mean surface temperature increases when P_{tot} increases and it reaches ~ 250 K when P_{tot} is 1 bar (Figure 7b). The ice cap reservoir was smaller than regolith and atmospheric reservoirs at any P_{tot} , which reaches the highest value of ~ 1 mbar when P_{tot} is ~ 100 mbar. The highest surface temperature was achieved at $\sim 40^\circ\text{S}$ when P_{tot} is between 20 and 600 mbar, while it is at the southern pole when P_{tot} is out of this range.

The calculations with respect to different solar luminosity under the present Martian orbital parameters and total exchangeable CO_2 are shown in Figure 7d–7f. The atmospheric and ice cap CO_2 reservoirs increase following the increase of the solar luminosity, while the regolith reservoir decreases slightly. The regolith reservoir was ~ 40 – 50 mbar at any solar luminosity explored in Figure 7d. The ice cap reservoir was lower than ~ 0.6 mbar regardless of the solar luminosity. The atmospheric $p\text{CO}_2$ was ~ 1 mbar when the relative solar luminosity was 0.7 (corresponding to ~ 4.5 Ga condition) and it increased to ~ 10 mbar when the relative solar luminosity was 1.2. The global annual mean surface temperature increases with respect to the increase of solar luminosity. It is ~ 190 K when the relative solar luminosity is 0.7 and it increases to ~ 220 K when the relative solar luminosity is 1.2. The solar luminosity did not strongly affect the latitude of the highest surface temperature.

The calculations with respect to different total exchangeable CO_2 and obliquity under the present solar luminosity are shown in Figure 8a. In this figure, the maximum P_{atm} that is possible in each condition is shown with colors. As investigated above, the changes in P_{atm} were controlled primarily by changes in P_{tot} when the permanent CO_2 ice does not exist, while obliquity does not strongly affect P_{atm} . When P_{tot} is sufficiently high, a climate mode without a permanent ice sheet can exist owing to the high atmospheric $p\text{CO}_2$ even under low obliquity conditions. Specifically, if obliquity is lower than $\sim 12^\circ$, the model expects that multiple climate modes can exist depending on the presence or absence of the permanent ice. Under the permanent ice solution, the atmospheric $p\text{CO}_2$ is similar to the values in the seasonal ice solution near the boundary of the multiple solutions.

In this case, the permanent ice exists only in the northern hemisphere, indicating that the formation of the southern CO₂ ice cap is important for the atmospheric collapse. The f_{hab} value is shown in Figure 8d. Even with high P_{tot} (1 bar) and high obliquity, the f_{hab} value is smaller than 15%, indicating the limited surface habitability in the Mars-like CO₂ system. When the obliquity is below 20°, f_{hab} is zero even when P_{tot} is 1 bar. Specifically, there is no latitudinal zone that is habitable throughout the year, and there is no season in which any latitude is habitable in our parameter space (Figure 8). These results indicate that the habitability on the surface of Mars would be limited. A larger atmospheric greenhouse effect than a 1-bar CO₂ atmosphere is necessary to keep the surface habitable as previously suggested (Pollack et al. 1987; Ramirez et al. 2014, 2020; Wordsworth et al. 2017; Kamada et al. 2020, 2021, 2022).

The responses of the Martian CO₂-driven system when eccentricity and precession angle from the vernal equinox are changed from the present Martian conditions are shown in Figures 5d–5f and 5g–5i, respectively. The distributions of the CO₂ reservoirs do not respond to the change in eccentricity, even under unrealistically high eccentricity (~ 0.4). The latitude with the highest surface temperature was $\sim 40^\circ\text{N}$ when eccentricity is zero, while it turns to $\sim 40^\circ\text{S}$ when eccentricity is over zero (Figure 5f). Higher eccentricity increases the maximum temperature, while the global mean surface temperature does not respond to eccentricity. When the precession angle from the vernal equinox is changed, the distributions of the CO₂ reservoirs do not respond to the change in eccentricity (Figure 5g). The latitude with the highest surface temperature, on the other hand, depends on the precession angle. This indicates that obliquity would have a dominant control in the atmospheric $p\text{CO}_2$ than eccentricity and precession. When the precession angle from the vernal equinox is $\sim 10^\circ$ – 180° , it is $\sim 30^\circ$ – 40°N , while it turns to $\sim 30^\circ$ – 40°S when the precession angle from the vernal equinox is $\sim 180^\circ$ – 360° .

We further show the results under different values of solar irradiance and total CO₂ mass on the climate system (Figure 8c). Calculations were conducted with respect to low obliquity value (10°). With the lower P_{tot} and solar luminosity, the atmospheric $p\text{CO}_2$ becomes low owing to the

accumulation of CO₂ ice. When P_{tot} is sufficiently high, the climate mode without permanent CO₂ ice can exist owing to the stronger greenhouse effect. This boundary is also dependent on the solar luminosity. With high solar luminosity, climate mode without permanent ice can be achieved with lower P_{tot} . The f_{hab} value is zero even with P_{tot} of 1 bar when the solar luminosity is below the present value, supporting the difficulty in sustaining the warm environment on early Mars only with CO₂.

Evolution of the Martian CO₂ system during the Noachian and Hesperian

The result of calculations with respect to different ages considering the changes in P_{tot} and solar luminosity in the history of Mars, the distribution of CO₂ is estimated in Figure 9 for four different obliquity values (10, 25.19, 45, and 60°). For the case with the present obliquity, the initial atmospheric $p\text{CO}_2$ at 3.8 Ga is ~0.2–0.3 bar, which was the largest reservoir of CO₂ (Figures 9a and 9b). The atmospheric $p\text{CO}_2$ decreases following the decline in P_{tot} caused by ion sputtering and photochemical escape and deposition of carbonates, while the changes in the CO₂ ice and regolith reservoirs do not respond strongly to the decline in P_{tot} . The decline in atmospheric $p\text{CO}_2$ ceases at ~3.0 Ga when the P_{tot} becomes close to the present value. Since then, the distribution of CO₂ has not varied strongly, indicating that the CO₂ system is less sensitive to the changes in the solar luminosity in the history of Mars. The overall characteristics of the responses are similar for the case with a higher obliquity value (45° and 60°). For the case of low obliquity (10°), the atmospheric $p\text{CO}_2$ was ~1 mbar at 3.8 Ga, resulting in a lower surface temperature. In this case, the mass of CO₂ ice gradually decreases until 1.0 Ga owing to the decline in P_{tot} and the increase in solar luminosity. The atmospheric $p\text{CO}_2$ drops down to ~0.3 mbar at ~3.0 Ga and it gradually increases following the increase in the solar luminosity. These results indicate that the values of obliquity are especially important in understanding the early history of Mars. Specifically, the atmospheric $p\text{CO}_2$ may fluctuate between >100 and <1 mbar on early Mars owing to the variation of obliquity. This means that the atmospheric collapse that results in the change in atmospheric $p\text{CO}_2$ with a factor of more than 100 could have occurred repeatedly following the obliquity cycle.

Conditions and timescales of the atmospheric collapse

The conditions for the atmospheric collapse under two different solar luminosities (75 and 100% of the present brightness) are shown in Figures 8b and 8a, respectively. When the solar luminosity is 75% (Figure 8b), the atmospheric collapse occurs only when the total exchangeable CO_2 becomes less than 0.3–0.6 bar when the initial state is set to the condition with high atmospheric $p\text{CO}_2$. With a larger total exchangeable CO_2 , the atmospheric collapse cannot occur owing to the greenhouse effect of atmospheric CO_2 . The atmospheric collapse also occurs when the obliquity becomes low. The critical obliquity increases up to $\sim 20^\circ$ following the increase of P_{tot} under a total exchangeable CO_2 below ~ 0.1 bar (Figure 8b). With a solar luminosity of 100 % (Figure 8a), the maximum values of both total exchangeable CO_2 and obliquity for the atmospheric collapse are smaller than for the case with 75 % solar luminosity. These results indicate that atmospheric collapse occurs more easily on early Mars than on present Mars. The Martian past obliquity would have transiently dropped below 22° in the Martian recent past (Laskar et al. 2004) (Figure 1a), which would have caused the atmospheric collapse on early Mars.

The time-dependent behavior of the atmosphere-ice cap system when the model is run under a transient variation of obliquity and the present solar luminosity is shown in Figure 10. When the obliquity drops below the critical value for the atmospheric collapse ($\sim 12^\circ$), the atmospheric $p\text{CO}_2$ suddenly decreases from the initial value (0.1 bar) to levels lower than 10^{-4} bar. After the collapse of the atmosphere, the atmosphere eventually starts to increase following the increase in the obliquity. The atmospheric $p\text{CO}_2$ returns to the initial value ~ 20 kyr after the timing of the lowest atmospheric $p\text{CO}_2$. These results show that the response timescale of the atmospheric collapse is well shorter than the variations of orbital parameters. This indicates that the atmospheric collapse would occur repeatedly given that the obliquity drops repeatedly below the critical level for the atmospheric collapse.

Discussion

In this study, we investigated the climate and habitability of Mars under dry conditions. We showed that once the Martian obliquity decreases below the threshold obliquity for the formation of the southern permanent ice, the atmospheric $p\text{CO}_2$ would decrease sharply, which corresponds to the atmospheric collapse (Soto et al. 2015). This boundary obliquity is lower than the reconstructed obliquity for the last 10 Myr, indicating that the atmospheric collapse would not have occurred in the last 10 Myr (Figure 1). A previous modeling study indicated that the layered CO_2 ice in the southern ice cap recorded periods of low obliquity in the recent past (Buhler et al. 2020; Buhler 2023). On the other hand, our model infers that the permanent CO_2 ice did not form in the recent past. This may suggest that the layered CO_2 ice formed regionally owing to the local topographic reliefs and developments of stationary waves or it may have formed in a more distant past. For a better constraint on the formation of the perennial CO_2 ice, investigations using three-dimensional models would be desirable (Soto et al. 2015). In the more distant past, variations of Martian obliquity are difficult to estimate owing to the chaotic behavior of orbital parameters, however, results of the ensemble of the estimates of the obliquity for the last 250 Myr exhibit periods with obliquity lower than 10° (Laskar et al., 2004). In such conditions, the atmospheric collapse would have occurred repeatedly on Mars.

Our result indicates that the atmospheric $p\text{CO}_2$ would have decreased following the decline in the total reservoir size of exchangeable CO_2 via ion sputtering and photochemical escape to space and/or deposition of carbonate. Therefore, the long-term history of the outgassing of CO_2 , escape of CO_2 , and the deposition of carbonate would be central to understanding Martian CO_2 distributions among the atmosphere, regolith, and ice caps. The carbonate deposition during the Noachian and Hesperian is highly uncertain. The estimate based on the exposure at Nili Fossae is 0.012 bar (Ehlmann et al. 2008; Edwards and Ehlmann 2015; Hu et al. 2015). The upper estimate based on the non-detectability of carbonate from orbital remote sensing data is 1.4 bar, assuming the 500 m thickness of carbonate-bearing crust, while this value would be down to 0.3 bar with a plausible carbonate content in the crust (Hu et al. 2015). The deposition of carbonate during the Amazonian is

estimated to be at most 7 mbar, based on the carbonate content in Martian dust and soil of the northern plain (Bandfield et al. 2003; Zuber et al. 2007; Watters et al. 2007; Sutter et al. 2012; Leshin et al. 2013; Hu et al. 2015). Similarly, the CO₂ outgassing flux on Martian history is affected by the outgassing scenarios and other factors such as the crustal redox state (Tajika and Sasaki 1996; Craddock and Greeley 2009; Grott et al. 2011). For a better constraint on the history of the Martian surface environment, further investigations of these processes together with the consideration of carbon isotopes would be beneficial for further investigation (Hu et al. 2015).

We showed that the surface habitability on Mars during the Amazonian is very limited. For such planets, life, if existed, may be suited for inhabiting subsurface environments because terrestrial microbes are not able to control their body temperature (Wright and Cooper 1981; Huey and Kingsolver 1989; Barnett and Olson 2022). Nevertheless, our results indicate that the surface becomes habitable at least seasonally with a wide range of total atmospheric $p\text{CO}_2$ when obliquity and/or eccentricity is high. The potential biospheric-atmospheric interactions with subsurface ecosystems would be a fruitful topic for future research. It is noteworthy that the actual habitability on Mars depends not only on climate and availability of water on the planetary surface but also on other factors such as supplies of essential elements, atmospheric redox state, and/or conditions suitable for the production of organic matter (Cockell 2014; Ehlmann et al. 2016; Koyama et al. 2021; Watanabe and Ozaki 2024; Ueno et al. 2024). Investigating the combination of these processes together with the advancement of future Mars missions for life detection (Jones 2018; Changela et al. 2021) would further help in understanding the habitability of Mars-like planets for future searches for signs of life on exoplanetary atmospheres.

Conclusions

The stability and habitability of the Martian CO₂-driven climate system were investigated in this study. We conducted numerical simulations under various conditions of orbital parameters, solar irradiance, and the total mass of surface exchangeable CO₂ using an energy-balanced climate model. The climate

solutions on Martian CO₂-driven climate systems depend on orbital parameters, solar luminosity, and the total CO₂ mass. Even considering the broad ranges of these parameters, the habitable condition on the Martian surface would be limited to high-latitude summer. The atmospheric collapse occurs when the obliquity is low, indicating that it would have occurred repeatedly in the history of Mars.

Acknowledgments

We thank H. Kurokawa for fruitful discussion. We also thank S. Kadoya for supporting the construction of the model. AK is supported by the Fusion Oriented REsearch for disruptive Science and Technology (FOREST) Program of the Japan Science and Technology Agency (JST) (Grant Number JPMJFR212U), the Japan Society for the Promotion of Science (JSPS) KAKENHI Grant Numbers JP23K13166.

Authorship statement

Conceptualization: YW; Methodology: YW; Software: YW; Investigation: YW, AK; Funding Acquisition: AK; Supervision: YW, ET; Visualization: YW; Writing – original draft: YW; Writing – review & editing: YW, ET, AK

Conflict of Interest Statement

The authors declare that they have no competing interest.

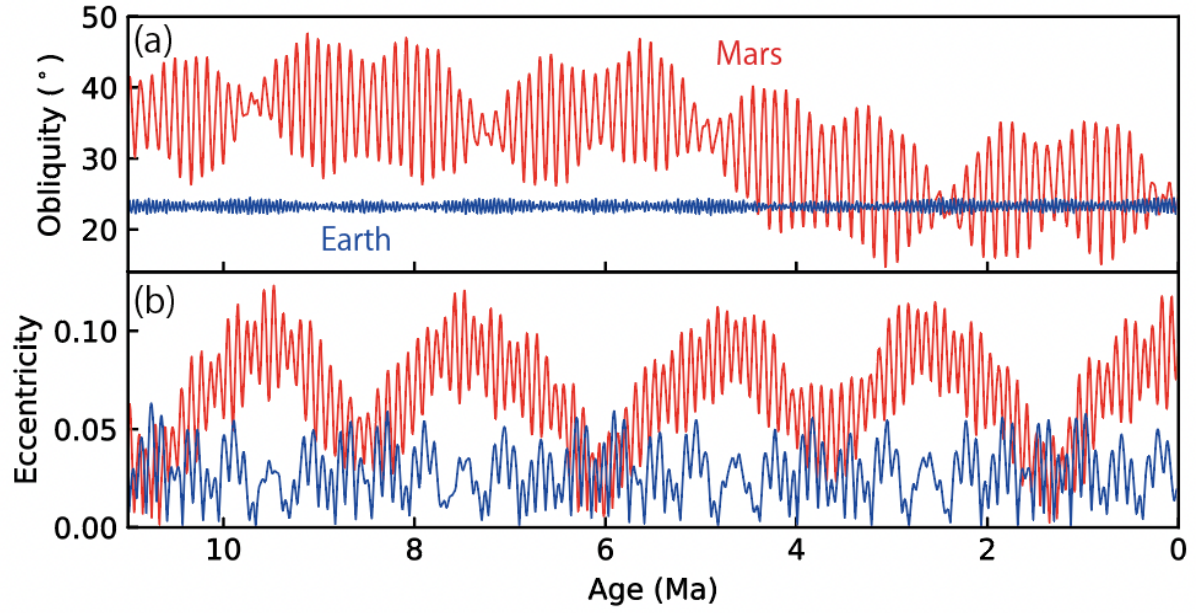


Figure 1. Variations of obliquity (a) and eccentricity (b) of Earth and Mars in the recent past (blue and red lines, respectively).

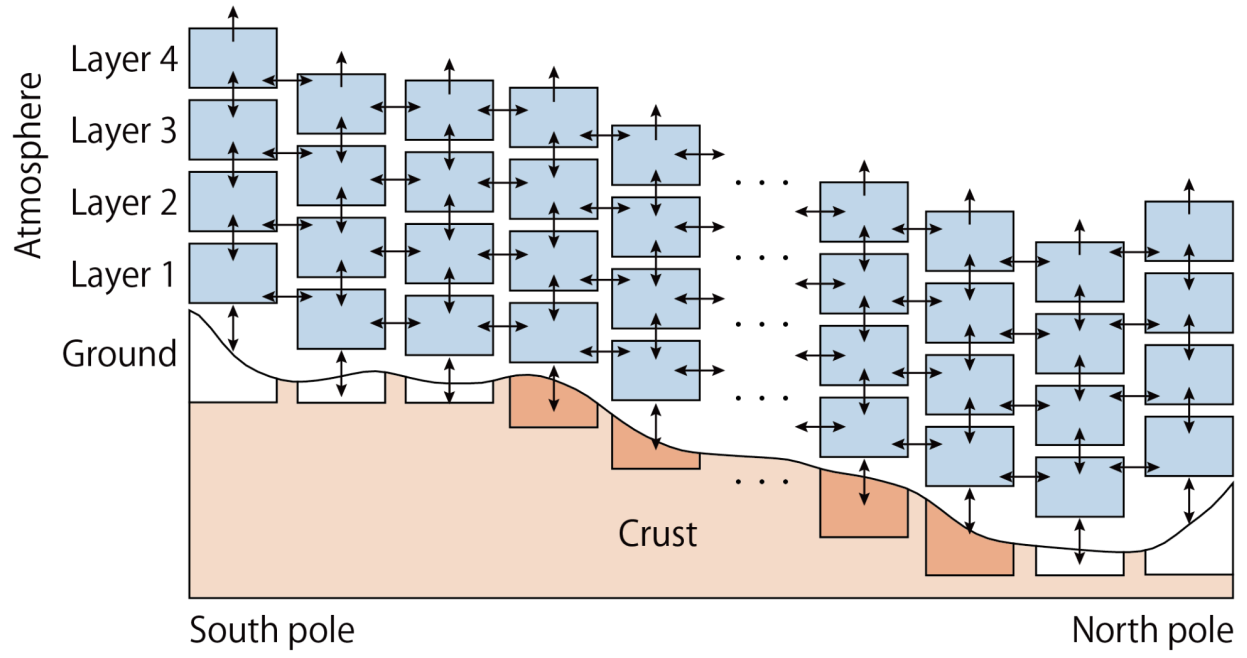


Figure 2. Schematic illustration of the energy-balanced climate model used in this study.

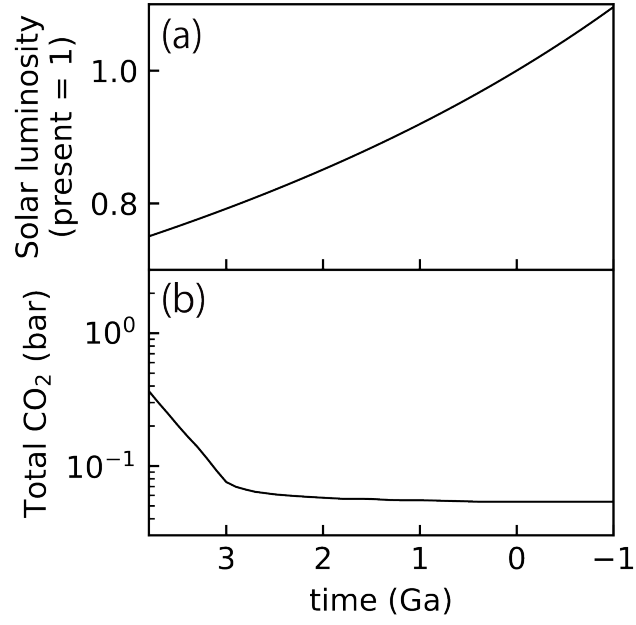


Figure 3. Evolutions of the solar luminosity (Gough, 1981) (a) and the total exchangeable CO₂ reservoir (atmosphere, ice, and regolith) (Hu et al., 2015) (b).

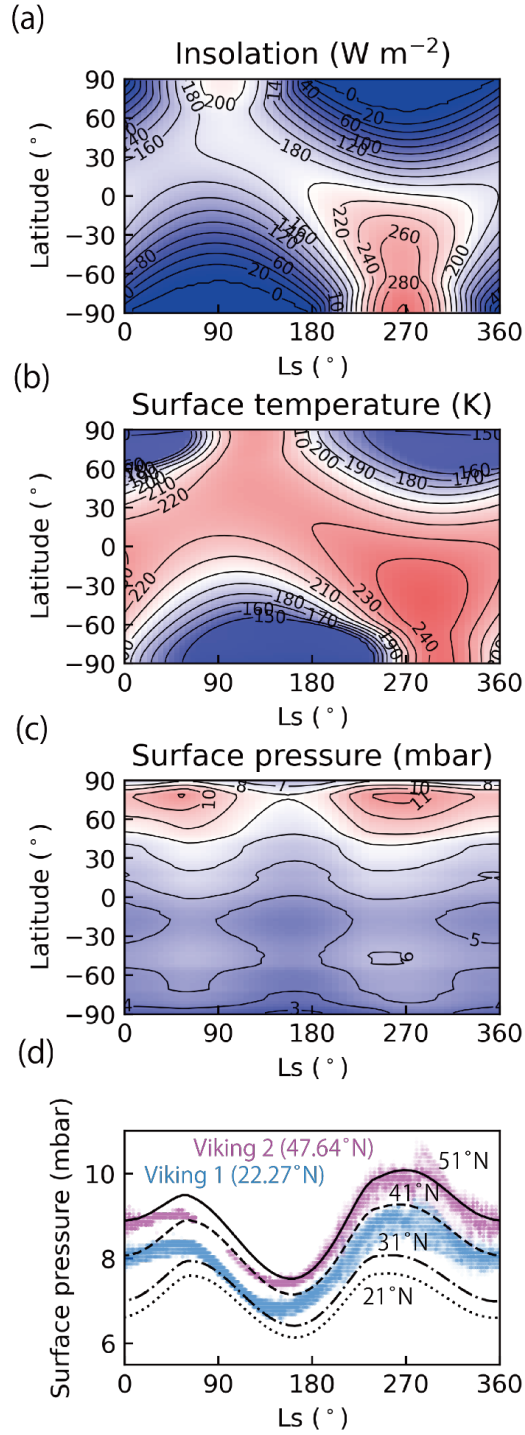


Figure 4. Seasonal and latitudinal variations of insolation (a), surface temperature (b), and surface pressure (c) simulated in our model assuming the present Mars condition. (d) Variations of the surface pressure simulated in our model assuming the present Mars condition at latitudes near the landing sites of Viking 1 and 2. Blue and purple represent observed variations of the surface pressure at landing sites) (Tillman, 1989).

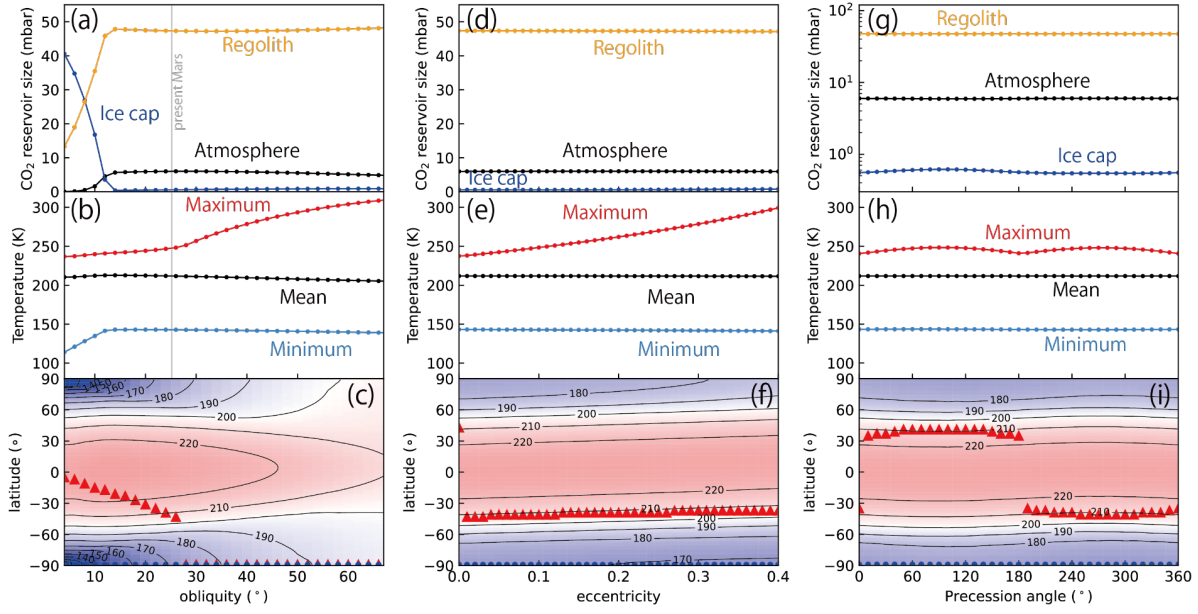


Figure 5. Distributions of CO₂ between the atmosphere, ice, and regolith (black, blue, and orange lines) (a, d, g), the maximum, mean, and minimum temperatures that are achieved on a planet (red, black, and blue lines, respectively) (b, e, h), and the latitudinal mean temperature (background color) and latitudes of maximum and minimum temperatures (red triangles and blue dots, respectively) (c, f, i) with respect to different obliquity (a–c), eccentricity (d–f), and precession angle from the vernal equinox (g–i).

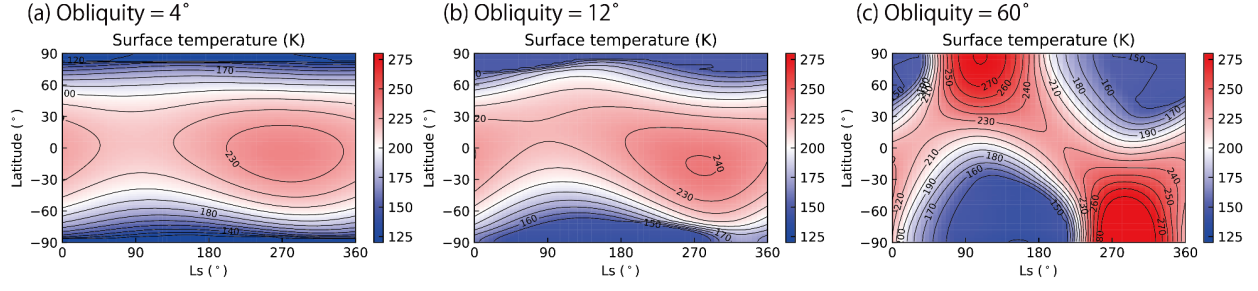


Figure 6. Seasonal and latitudinal variations of the surface temperature simulated with different obliquity (4° , 12° , and 60° for a, b, and c, respectively).

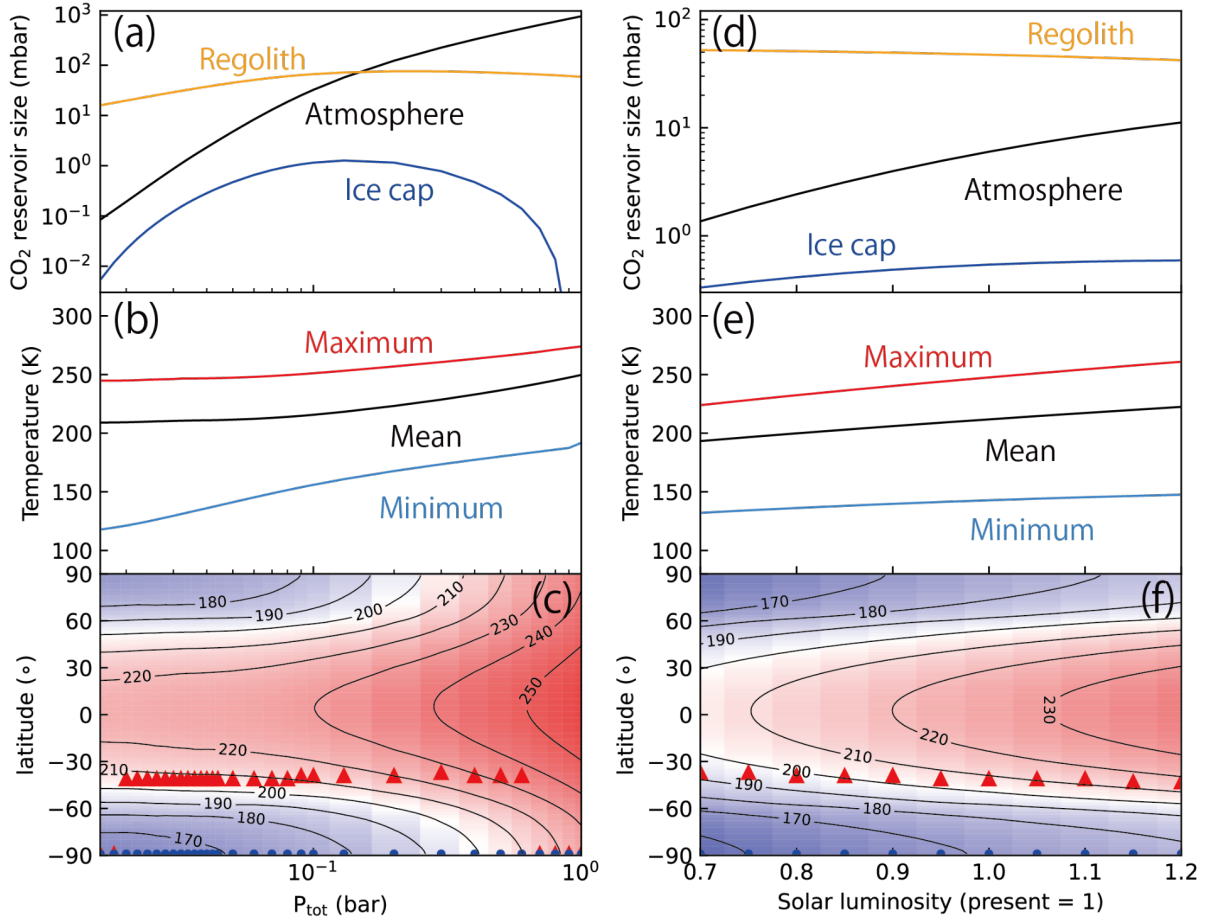


Figure 7. Distributions of CO₂ between the atmosphere, ice, and regolith (black, blue, and orange lines) (a, d), the maximum, mean, and minimum temperatures that are achieved on a planet (red, black, and blue lines, respectively) (b, e), and the latitudinal mean temperature (background color) and latitudes of maximum and minimum temperatures (red triangles and blue dots, respectively) (c, f) with respect to different total exchangeable CO₂ (P_{tot}) (a, b) and different solar luminosity (present = 1) (c, d). Calculations are conducted with the present Martian orbital parameters.

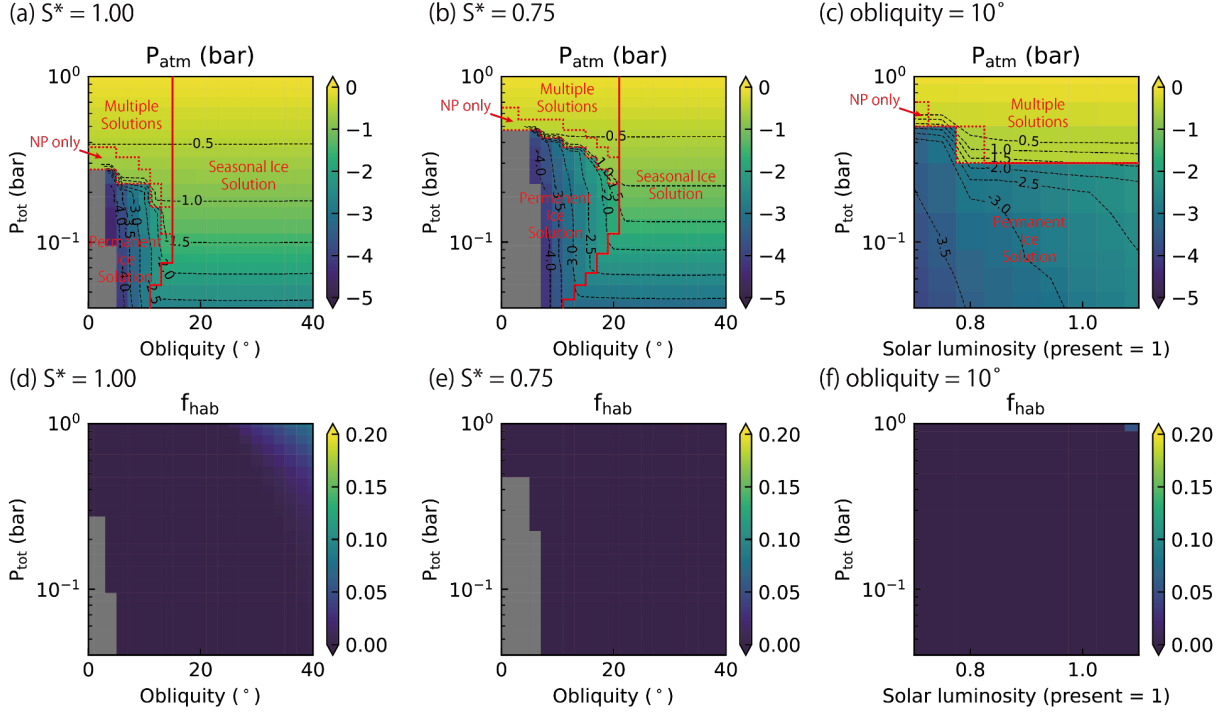


Figure 8. CO₂ reservoir sizes of the atmosphere (P_{atm}) (a–c), and the fractional habitability (f_{hab}) (d–f) calculated with respect to different obliquity and total exchangeable reservoir size (P_{tot}) under present solar luminosity (a, d), different solar luminosity and P_{tot} under an obliquity of 10° (b, e), and different obliquity and P_{tot} under solar luminosity of 0.75 times relative to the present value (c, f). The region “NP only” represents the solution with the permanent ice only at the north pole. The P_{atm} values shown in a, b, and c are the maximum value that is possible in each condition.

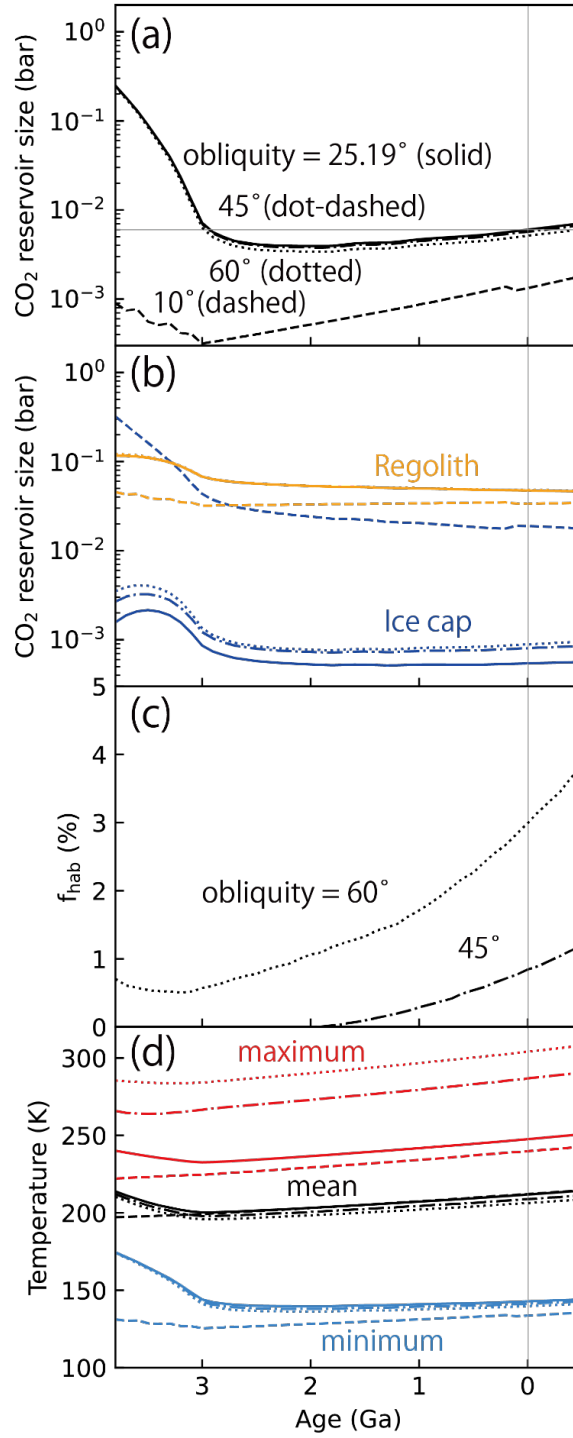


Figure 9. Evolutions of the exchangeable reservoirs and climate of Mars. (a) Atmospheric $p\text{CO}_2$, (b) ice and regolith reservoirs, (c) fractional habitability, and (d) maximum, mean, and minimum temperatures that are achieved on Mars. Calculations were conducted with respect to four obliquity values (10, 25.19, 45, and 60°; dashed, solid, dot-dashed, and dotted lines, respectively).

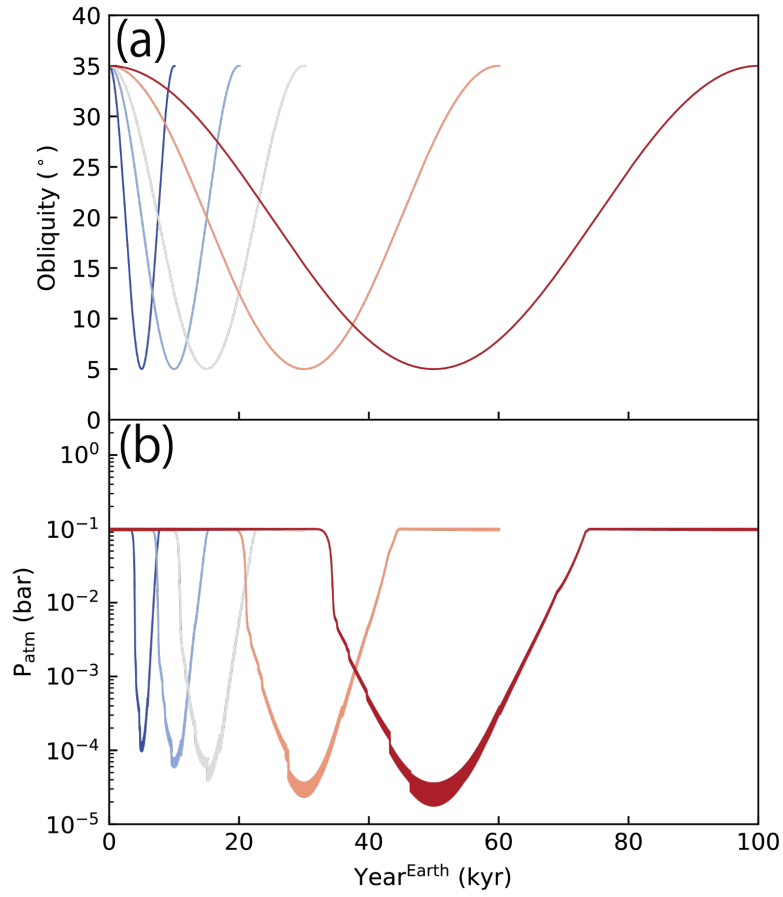


Figure 10. Time-dependent response of the Mars-like atmosphere-ice cap system to variations of obliquity forcing with different periodicities. (a) Variations of the obliquity forcing and (b) and corresponding variations of the Mars-like atmosphere-ice cap system are shown with solid lines. Colors represent the different periodicity of the variations of obliquity assumed in each calculation.

References

- Abe-Ouchi A, Saito F, Kawamura K, et al (2013) Insolation-driven 100,000-year glacial cycles and hysteresis of ice-sheet volume. *Nature* 500:190–193
- Bandfield JL, Glotch TD, Christensen PR (2003) Spectroscopic identification of carbonate minerals in the martian dust. *Science* 301:1084–1087
- Barnett MN, Olson SL (2022) Moderately High Obliquity Promotes Biospheric Oxygenation. *The Planetary Science Journal* 3:132
- Batalha NE, Kopparapu RK, Haqq-Misra J, Kasting JF (2016) Climate cycling on early Mars caused by the carbonate–silicate cycle. *Earth Planet Sci Lett* 455:7–13
- Becerra P, Byrne S, Sori MM, et al (2016) Stratigraphy of the north polar layered deposits of Mars from high-resolution topography. *J Geophys Res Planets* 121:1445–1471
- Becerra P, Sori MM, Byrne S (2017) Signals of astronomical climate forcing in the exposure topography of the North Polar Layered Deposits of Mars. *Geophys Res Lett* 44:62–70
- Becerra P, Sori MM, Thomas N, et al (2019) Timescales of the climate record in the south polar ice cap of mars. *Geophys Res Lett* 46:7268–7277
- Bernhardt H, Reiss D, Ivanov M, et al (2019) The banded terrain on northwestern Hellas Planitia: New observations and insights into its possible formation. *Icarus* 321:171–188
- Bierson CJ, Phillips RJ, Smith IB, et al (2016) Stratigraphy and evolution of the buried CO₂ deposit in the Martian south polar cap. *Geophysical Research Letters* 43:4172–4179
- Bramson AM, Byrne S, Bapst J (2017) Preservation of midlatitude ice sheets on mars: Mars midlatitude ice sheet preservation. *J Geophys Res Planets* 122:2250–2266
- Buhler PB (2023) A 510,000-Year Record of Mars’ Climate. *Geophys Res Lett* 50:e2022GL101752
- Buhler PB, Ingersoll AP, Piqueux S, et al (2020) Coevolution of Mars’s atmosphere and massive south polar CO₂ ice deposit. *Nature Astronomy* 4:364–371
- Buhler PB, Piqueux S (2021) Obliquity-Driven CO₂ Exchange Between Mars’ Atmosphere, Regolith, and Polar Cap. *Journal of Geophysical Research: Planets* 126:e2020JE006759
- Byrne S (2009) The Polar Deposits of Mars. *Annu Rev Earth Planet Sci* 37:535–560
- Changela HG, Chatzitheodoridis E, Antunes A, et al (2021) Mars: new insights and unresolved questions. *Int J Astrobiology* 20:394–426
- Citron RI, Manga M, Hemingway DJ (2018) Timing of oceans on Mars from shoreline deformation. *Nature* 555:643–646
- Cockell CS (2014) Trajectories of martian habitability. *Astrobiology* 14:182–203
- Conway SJ, Harrison TN, Soare RJ, et al (2019) New slope-normalized global gully density and orientation maps for Mars. *Geol Soc Spec Publ* 467:187–197

- Costard F, Forget F, Mangold N, Peulvast JP (2002) Formation of recent martian debris flows by melting of near-surface ground ice at high obliquity. *Science* 295:110–113
- Craddock RA, Greeley R (2009) Minimum estimates of the amount and timing of gases released into the martian atmosphere from volcanic eruptions. *Icarus* 204:512–526
- Dundas CM, Bramson AM, Ojha L, et al (2018) Exposed subsurface ice sheets in the Martian mid-latitudes. *Science* 359:199–201
- Edwards CS, Ehlmann BL (2015) Carbon sequestration on Mars. *Geology* 43:863–866
- Ehlmann BL, Anderson FS, Andrews-Hanna J, et al (2016) The sustainability of habitability on terrestrial planets: Insights, questions, and needed measurements from Mars for understanding the evolution of Earth-like worlds: Mars and Terrestrial Planet Habitability. *J Geophys Res Planets* 121:1927–1961
- Ehlmann BL, Mustard JF, Murchie SL, et al (2008) Orbital identification of carbonate-bearing rocks on Mars. *Science* 322:1828–1832
- Fanale FP, Cannon WA (1974) Exchange of adsorbed H₂O and CO₂ between the regolith and atmosphere of Mars caused by changes in surface insolation. *J Geophys Res* 79:3397–3402
- Fanale FP, Salvail JR (1982) Mars" The Regolith-Atmosphere-Cap System and Climate Change I. *Icarus* 50:381–407
- Feulner G (2012) The faint young Sun problem. *Reviews of Geophysics* 50:
- Forget F, Haberle RM, Montmessin F, et al (2006) Formation of glaciers on Mars by atmospheric precipitation at high obliquity. *Science* 311:368–371
- Gary-Bicas CE, Hayne PO, Horvath T, et al (2020) Asymmetries in snowfall, emissivity, and albedo of mars' seasonal polar caps: Mars climate sounder observations. *J Geophys Res Planets* 125:e2019JE006150
- Gierasch PJ, Toon OB (1973) Atmospheric Pressure Variation and the Climate of Mars. *J Atmos Sci* 30:1502–1508
- Gough DO (1981) Solar Interior Structure and Luminosity Variations. In: Domingo V (ed) *Physics of Solar Variations*. Springer Netherlands, Dordrecht, pp 21–34
- Grott M, Morschhauser A, Breuer D, Hauber E (2011) Volcanic outgassing of CO₂ and H₂O on Mars. *Earth Planet Sci Lett* 308:391–400
- Haberle RM, Todd Clancy R, Forget F, et al (2017) *The Atmosphere and Climate of Mars*. Cambridge University Press
- Haberle RM, Tyler D, McKay CP, Davis WL (1994) A model for the evolution of CO₂ on Mars. *Icarus* 109:102–120
- Hays JD, Imbrie J, Shackleton NJ (1976) Variations in the earth's orbit: Pacemaker of the ice ages. *Science* 194:1121–1132
- Hayworth BPC, Kopparapu RK, Haqq-Misra J, et al (2020) Warming early Mars with climate

- cycling: The effect of CO₂-H₂ collision-induced absorption. *Icarus* 345:113770
- Head JW 3rd, Hiesinger H, Ivanov MA, et al (1999) Possible ancient oceans on Mars: evidence from Mars Orbiter Laser Altimeter data. *Science* 286:2134–2137
- Head JW, Mustard JF, Kreslavsky MA, et al (2003) Recent ice ages on Mars. *Nature* 426:797–802
- Hoffert MI, Callegari AJ, Hsieh CT, Ziegler W (1981) Liquid water on Mars: An energy balance climate model for CO₂/H₂O atmospheres. *Icarus* 47:112–129
- Huey RB, Kingsolver JG (1989) Evolution of thermal sensitivity of ectotherm performance. *Trends Ecol Evol* 4:131–135
- Hu R, Kass DM, Ehlmann BL, Yung YL (2015) Tracing the fate of carbon and the atmospheric evolution of Mars. *Nat Commun* 6:10003
- Huybers P (2011) Combined obliquity and precession pacing of late Pleistocene deglaciations. *Nature* 480:229–232
- Hvidberg CS, Fishbaugh KE, Winstrup M, et al (2012) Reading the climate record of the martian polar layered deposits. *Icarus* 221:405–419
- Jakosky BM, Edwards CS (2018) Inventory of CO₂ available for terraforming Mars. *Nature Astronomy* 2:634–639
- Jakosky BM, Pepin RO, Johnson RE, Fox JL (1994) Mars Atmospheric Loss and Isotopic Fractionation by Solar-Wind-Induced Sputtering and Photochemical Escape. *Icarus* 111:271–288
- Jones EG (2018) Shallow transient liquid water environments on present-day mars, and their implications for life. *Acta Astronaut* 146:144–150
- Kahn R (1985) The evolution of CO₂ on Mars. *Icarus* 62:175–190
- Kamada A, Kuroda T, Kasaba Y, et al (2020) A coupled atmosphere–hydrosphere global climate model of early Mars: A “cool and wet” scenario for the formation of water channels. *Icarus* 338:113567
- Kamada A, Kuroda T, Kasaba Y, et al (2021) Global climate and river transport simulations of early Mars around the Noachian and Hesperian boundary. *Icarus* 368:114618
- Kamada A, Kuroda T, Kodama T, et al (2022) Evolution of ice sheets on early Mars with subglacial river systems. *Icarus* 385:115117
- Kasting JF (1991) CO₂ condensation and the climate of early Mars. *Icarus* 94:1–13
- Kieffer HH (1979) Mars south polar spring and summer temperatures: A residual CO₂ frost. *Journal of Geophysical Research: Solid Earth* 84:8263–8288
- Kieffer HH, Zent AP (1992) Quasi-periodic climate change on Mars. In: Kieffer HH (ed) *Mars*. University of Arizona Press, pp 1180–1218
- Kite ES, Conway S (2024) Geological evidence for multiple climate transitions on Early Mars. *Nat Geosci* 17:10–19

- Kite ES, Gao P, Goldblatt C, et al (2017) Methane bursts as a trigger for intermittent lake-forming climates on post-Noachian Mars. *Nat Geosci* 10:737–740
- Kite ES, Halevy I, Kahre MA, et al (2013) Seasonal melting and the formation of sedimentary rocks on Mars, with predictions for the Gale Crater mound. *Icarus* 223:181–210
- Koyama S, Terada N, Nakagawa H, et al (2021) Stability of Atmospheric Redox States of Early Mars Inferred from Time Response of the Regulation of H and O Losses. *ApJ* 912:135
- Kreslavsky MA, Head JW (2005) Mars at very low obliquity: Atmospheric collapse and the fate of volatiles. *Geophys Res Lett* 32:
- Kurahashi-Nakamura T, Tajika E (2006) Atmospheric collapse and transport of carbon dioxide into the subsurface on early Mars. *Geophys Res Lett* 33:
- Lalich DE, Holt JW (2017) New Martian climate constraints from radar reflectivity within the north polar layered deposits: Martian Radar and Climate Constraints. *Geophys Res Lett* 44:657–664
- Lalich DE, Holt JW, Smith IB (2019) Radar reflectivity as a proxy for the dust content of individual layers in the martian north polar layered deposits. *J Geophys Res Planets* 124:1690–1703
- Laskar J, Correia ACM, Gastineau M, et al (2004) Long term evolution and chaotic diffusion of the insolation quantities of Mars. *Icarus* 170:343–364
- Leshin LA, Mahaffy PR, Webster CR, et al (2013) Volatile, isotope, and organic analysis of martian fines with the Mars Curiosity rover. *Science* 341:1238937
- Manning CV, Bierson C, Putzig NE, McKay CP (2019) The formation and stability of buried polar CO₂ deposits on Mars. *Icarus* 317:509–517
- Manning CV, McKay CP, Zahnle KJ (2006) Thick and thin models of the evolution of carbon dioxide on Mars. *Icarus* 180:38–59
- McKay CP, Toon OB, Kasting JF (1991) Making Mars habitable. *Nature* 352:489–496
- Nakamura T, Tajika E (2003) Climate change of Mars-like planets due to obliquity variations: implications for Mars. *Geophys Res Lett* 30:
- Nakamura T, Tajika E (2001) Stability and evolution of the climate system of Mars. *Earth Planets Space* 53:851–859
- Nakamura T, Tajika E (2002) Stability of the Martian climate system under the seasonal change condition of solar radiation. *Journal of Geophysical Research: Planets* 107:
- Pierrehumbert RT, Erlick C (1998) On the scattering greenhouse effect of CO₂ ice clouds. *J Atmos Sci* 55:1897–1903
- Piqueux S, Kleinböhl A, Hayne PO, et al (2015) Variability of the martian seasonal CO₂ cap extent over eight Mars Years. *Icarus* 251:164–180
- Pollack JB, Haberle RM, Murphy JR, et al (1993) Simulations of the general circulation of the Martian Atmosphere: 2. Seasonal pressure variations. *J Geophys Res* 98:3149–3181
- Pollack JB, Haberle RM, Schaeffer J, Lee H (1990) Simulations of the general circulation of the

Martian atmosphere: 1. Polar processes. *J Geophys Res* 95:1447–1473

Pollack JB, Kasting JF, Richardson SM, Poliakoff K (1987) The case for a wet, warm climate on early Mars. *Icarus* 71:203–224

Pollack JB, Leovy CB, Greiman PW, Mintz Y (1981) A Martian General Circulation Experiment with Large Topography. *J Atmos Sci* 38:3–29

Ramirez RM, Craddock RA, Usui T (2020) Climate simulations of early mars with estimated precipitation, runoff, and erosion rates. *J Geophys Res Planets* 125:e2019JE006160

Ramirez RM, Kopparapu R, Zugger ME, et al (2014) Warming early Mars with CO₂ and H₂. *Nat Geosci* 7:59–63

Rapin W, Dromart G, Clark BC, et al (2023) Sustained wet-dry cycling on early Mars. *Nature* 620:299–302

Raymo ME (1997) The timing of major climate terminations. *Paleoceanography* 12:577–585

Schon SC, Head JW, Milliken RE (2009) A recent ice age on Mars: Evidence for climate oscillations from regional layering in mid-latitude mantling deposits. *Geophys Res Lett* 36:

Smith DE, Zuber MT, Frey HV, Garvin JB (2001) Mars Orbiter Laser Altimeter: Experiment summary after the first year of global mapping of Mars. *Journal of Geophysical Research: Planets* 106:23689–23722

Smith IB, Putzig NE, Holt JW, Phillips RJ (2016) An ice age recorded in the polar deposits of Mars. *Science* 352:1075–1078

Soto A, Mischna M, Schneider T, et al (2015) Martian atmospheric collapse: Idealized GCM studies. *Icarus* 250:553–569

Spiegel DS, Menou K, Scharf CA (2008) Habitable Climates. *The Astrophysical Journal* 681:1609–1623

Stone PH (1972) A Simplified Radiative-Dynamical Model for the Static Stability of Rotating Atmospheres. *J Atmos Sci* 29:405–418

Sutter B, Boynton WV, Ming DW, et al (2012) The detection of carbonate in the martian soil at the Phoenix Landing site: A laboratory investigation and comparison with the Thermal and Evolved Gas Analyzer (TEGA) data. *Icarus* 218:290–296

Tajika E, Sasaki S (1996) Magma generation on Mars constrained from an ⁴⁰Ar degassing model. *J Geophys Res* 101:7543–7554

Tillman, J.E. (1989) VL1/VL2-M-MET-3-P-V1.0, NASA Planetary Data System.

Titus TN, Cushing GE (2014) Monitoring the Mars Polar Caps During Mars Years 24–28. 45th Lunar and Planetary Science Conference, p 2177

Toon OB, Pollack JB, Ward W, et al (1980) The astronomical theory of climatic change on Mars. *Icarus* 44:552–607

Ueno Y, Schmidt JA, Johnson MS, et al (2024) Synthesis of ¹³C-depleted organic matter from CO

in a reducing early Martian atmosphere. *Nat Geosci* 17:503–507

Walker JCG, Hays PB, Kasting JF (1981) A negative feedback mechanism for the long-term stabilization of Earth's surface temperature. *J Geophys Res* 86:9776

Watanabe Y, Abe-Ouchi A, Saito F, et al (2023) Astronomical forcing shaped the timing of early Pleistocene glacial cycles. *Communications Earth & Environment* 4:1–11

Watanabe Y, Ozaki K (2024) Relative abundances of CO₂, CO, and CH₄ in atmospheres of Earth-like lifeless planets. *Astrophys J* 961:1

Watters TR, Campbell B, Carter L, et al (2007) Radar sounding of the Medusae Fossae Formation Mars: equatorial ice or dry, low-density deposits? *Science* 318:1125–1128

Wood SE, Paige DA (1992) Modeling the Martian seasonal CO₂ cycle 1. Fitting the Viking Lander pressure curves. *Icarus* 99:1–14

Wordsworth R, Kalugina Y, Lokshtanov S, et al (2017) Transient reducing greenhouse warming on early Mars. *Geophys Res Lett* 44:665–671

Wright RK, Cooper EL (1981) Temperature effects on ectotherm immune responses. *Dev Comp Immunol* 5:117–122

Yokohata T, Odaka M, Kuramoto K (2002) Role of H₂O and CO₂ Ices in Martian Climate Changes. *Icarus* 159:439–448

Zent AP, Quinn RC (1995) Simultaneous adsorption of CO₂ and H₂O under Mars-like conditions and application to the evolution of the Martian climate. *J Geophys Res* 100:5341–5349

Zuber MT, Phillips RJ, Andrews-Hanna JC, et al (2007) Density of Mars' south polar layered deposits. *Science* 317:1718–1719

Zuber MT, Smith DE, Solomon SC, et al (1992) The Mars Observer laser altimeter investigation. *J Geophys Res* 97:7781